Journal of Advanced Research 45 (2023) 59–71

Contents lists available at ScienceDirect

Journal of Advanced Research

journal homepage: www.elsevier.com/locate/jare

Original Article

Turning chiral peptides into a racemic supraparticle to induce the self-degradation of MDM2

Wenguang Yang [a,1], Wenjia Liu [b,1,*], Xiang Li [c,1], Jin Yan [b,*], Wangxiao He [a,d,*]

[a] Department of Medical Oncology and Department of Talent Highland, The First Affiliated Hospital of Xi'an Jiao Tong University, Xi'an 710061, China
[b] National & Local Joint Engineering Research Center of Biodiagnosis and Biotherapy, The Second Affiliated Hospital of Xi'an Jiaotong University, Xi'an 710004, China
[c] School of Pharmacy, Second Military Medical University, Shanghai 200433, China
[d] Institute for Stem Cell & Regenerative Medicine, The Second Affiliated Hospital of Xi'an Jiaotong University, Xi'an 710004, China

HIGHLIGHTS

- A mild and simple self-assembly strategy for the construction of peptide-derived chiral supramolecular nanomedicine.
- A D-peptide as MDM2 Self-Degradation catalysts to induce the self-degradation of a carcinogenic E3 Ubiquitin ligase termed MDM2.
- MSDNc preponderantly suppressed the tumor progression and synergized the tumor immunotherapy.

GRAPHICAL ABSTRACT

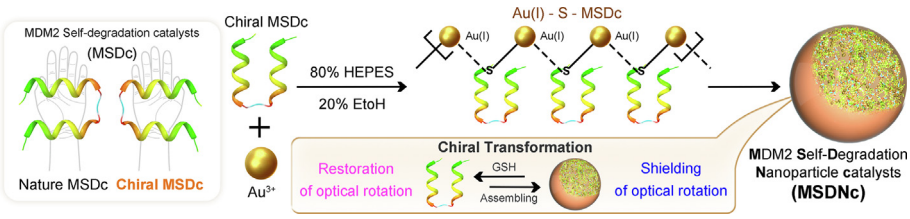

ARTICLE INFO

Article history:
Received 24 February 2022
Revised 4 May 2022
Accepted 24 May 2022
Available online 3 June 2022

Keywords:
Peptide
Chiral molecule
Supramolecular self-assembly
D-enantiomeric peptide
Cancer therapy

ABSTRACT

Introduction: Chirality is immanent in nature, and chiral molecules can achieve their pharmacological action through chiral matching with biomolecules and molecular conformation recognition.
Objectives: Clinical translation of chiral therapeutics, particularly chiral peptide molecules, has been hampered by their unsatisfactory pharmaceutical properties.
Methods: A mild and simple self-assembly strategy was developed here for the construction of peptide-derived chiral supramolecular nanomedicine with suitable pharmaceutical properties. In this proof-of-concept study, we design a D-peptide as MDM2 Self-Degradation catalysts (MSDc) to induce the self-degradation of a carcinogenic E3 Ubiquitin ligase termed MDM2. Exploiting a metal coordination between mercaptan in peptides and trivalent gold ion, chiral MSDc was self-assembled into a racemic supraparticle (MSDNc) that eliminated the consume from the T-lymphocyte/macrophage phagocytose in circulation.
Results: Expectedly, MSDNc down-regulated MDM2 in more action than its L-enantiomer termed ^{Ctrl}MSDNc. More importantly, MSDNc preponderantly suppressed the tumor progression and synergized the tumor immunotherapy in allograft model of melanoma through p53 restoration in comparison to ^{Ctrl}MSDNc.
Conclusion: Collectively, this work not only developed a secure and efficient therapeutic agent targeting MDM2 with the potential of clinical translation, but also provided a feasible and biocompatible strategy for the construction of peptide supraparticle and expanded the application of chiral therapeutic and homo-PROTAC to peptide-derived chiral supramolecular nanomedicine.

Peer review under responsibility of Cairo University.
* Corresponding authors.
E-mail addresses: wenjialiu@xjtu.edu.cn (W. Liu), yanjin19920602@xjtu.edu.cn (J. Yan), hewangxiao5366@xjtu.edu.cn (W. He).
[1] These authors contributed equally.

https://doi.org/10.1016/j.jare.2022.05.009
2090-1232/

Introduction

Chirality, a class of enantiotropy meaning that two molecules have identical elemental compositions but are non-superimposable on their mirror images, is immanent in nature and inherent in every biological system [1,2]. Interestingly, evolution selected L-form peptide/protein and D-form sugars/nucleic acid as the main components in most living organisms [3,4]. This homochirality of biomolecules and the subsequent lack of racemate is a striking property that serve as the important role for biological function [5,6]. By using this molecular asymmetry in life activities, chiral molecules can achieve their pharmacological action through chiral matching with biomolecules and molecular conformation recognition [7,8]. As a result, a growing number of drugs were emerged in an enantiomerically pure form, which exhibited the excellent biological action and the expectant therapeutic safety [7,8].

While many successes have been achieved in developing chiral therapeutics by small molecular compound, significant challenges remain regarding to clinical translation of therapeutic chiral peptides [9,10]. Peptide molecules, both L-enantiomer and D-enantiomer, can mimic the topological structure of large proteins, so as to be a class of modulators to regulate protein–protein interactions (PPIs) [11,12]. In contrast to natural L-peptide, D-peptide, or addressed chiral peptide, have two intrinsic advantage as anticancer therapeutic agents: 1) the excellent proteolytic resistance because of the L- enantiomeric selectivity of peptidase [10,13,14], and 2) the enhanced uptake by cancer cells due to the strengthened affinity to lipid layers composed of phospholipids and cholesterol [5]. Even so, none of the chiral peptide that targets intracellular PPIs has been approved for clinical application, presumably because of its inefficacious accumulation in sickly tissues and unsatisfactory stability in blood circulation [15]. Ultimately, both of the weaknesses of D-peptide were attributed to the undesired consume from the T-lymphocyte/macrophage phagocytose in circulation and the quick remove by kidney [15,16]. Therefore, there is a compelling need to develop new strategies for overcoming the pharmaceutical obstacles of D-peptides, extending the chiral therapeutics from small-molecular compounds to peptides.

Fortunately, both L-enantiomeric and D-enantiomeric peptides can be building blocks to self-assemble into nanostructures with biological action, exploiting a variety of non-covalent weak interactions such hydrogen bonding, hydrophobic force, coulombian force and metal coordination [6,17]. Moreover, chiral supramolecular nanomedicines have showed enormous potential to overcome the deficiency of chiral molecule including but not limited to the insufficient stability in circulation, the undesired uptakes by immune cell and the limited accumulation in the site of interest such as tumor [18,19]. Nevertheless, the physiological and biochemical role of supramolecular chirality, particularly those derived from peptide, in life activities have not been unclosed and yet [5,20]. Besides, though some success has been achieved in the construction of supramolecular nanomedicines by chiral peptide, it remains a challenge to endow them with the controllability of chirality transfer and manufacture them in a larger scale [21–23].

Herein, to design peptide-derived chiral supramolecular nanomedicine with suitable pharmaceutical properties for clinical translation, a mild and simple self-assembly strategy was developed to turn the building block - chiral peptide- into a spherical supraparticle exploiting a metal coordination between mercaptan in peptides and trivalent gold ion. Because of the flexibility of the gold-sulfur interface, this chiral gold spherical supraparticle undergone racemization, which eliminated the consume from the T-lymphocyte/macrophage phagocytose in circulation of D-enantiomeric peptides. In this proof-of-concept study, we design a D-peptide as MDM2 Self-Degradation catalysts (MSDc) to induce the self-degradation of a carcinogenic E3 Ubiquitin ligase termed MDM2 through the chemically linked dimerization of a MDM2 binding D-peptide. Self-assembling MSDc into a spherical supraparticle termed MDM2 Self-Degradation Nanocatalysts (MSDNc) resulted in the potently homo-degradation of MDM2. To further revealed the physiological and biochemical role of this supramolecular chirality *in vivo* and *in vitro*, the L-enantiomer of MSDc (^{Ctrl}MSDc) with the same capacity to catalyze MDM2 homo-degradation was designed and self-assembled into ^{Ctrl}-MSDNc for comparative study to MSDNc. As expected, in more action than ^{Ctrl}MSDNc, MSDNc down-regulated MDM2 and subsequent suppressed the tumor progression *in vivo* and *in vitro* through p53 restoration. As it were, our work not only developed a secure and efficient therapeutic agent targeting MDM2 with the potential of clinical translation, but also provided a feasible and biocompatible strategy for the construction of peptide supraparticle and expanded the application of chiral therapeutic and homo-PROTAC to peptide-derived chiral supramolecular nanomedicine.

Results

Preparation and characterization of MSDNc.

Human murine double minute-2 (MDM2) is one of the pivotal suppressors to restrain the anti-cancer biological function of p53, and has been recognized as a viable target for drug discovery [24–27]. Moreover, MDM2 is a E3 Ubiquitin ligase and thus has the potential to be self- degraded by homo-proteolysis targeting chimeras (PROTACs) [28]. To design this sub-stoichiometric MDM2 Self-Degradation catalysts (MSDc), an identical chiral MDM2 affinity peptide [10,29–31] was dimerized by a triethylene glycol linker as diagramed in Fig. 1. In addition, for supramolecular assembly with trivalent gold ions, a hydrophilic D-enantiomeric arginine residue and a thiol-containing D-enantiomeric cysteine residue were introduced into the C-terminus of MSDc, and this chiral peptide can be synthesized by solid-phase peptide synthesis (SPSS) [32–35] in high yield (>75%) and purity (>95%) (Figure S1A&B). For comparative study of chirality, the L-enantiomer of MSDc (^{Ctrl}MSDc) with the same capacity to catalyze MDM2 homo-degradation was synthesized in the same chemical strategy, suggesting the high yield (>75%) and purity (>95%) via HPLC and ESI-MASS (Figure S1C&D). In addition, the benzene ring absorption peak at 280 nm in the UV spectra of MSDc and ^{Ctrl}MSDc have verified the successful preparation of peptides (Figure S1E), which was also proved by the prominent amide bond absorption peaks in the FTIR spectra (Figure S1F). And the abundant side chain functional groups in the H1 NMR spectra verified the successful preparation of MSDc and ^{Ctrl}MSDc (Figure S1G).The optical rotation was proved by their circular dichroism (CD), in which the CD spectrometer of MSDc and ^{Ctrl}MSDc showed characteristic peaks of α-helical structure at 195 nm, 208 nm, and 222 nm, and appeared X-axis symmetry (Fig. 2A).[10].

MSDc-derived supraparticles termed MSDNc are prepared by a mild and simple self-assembly strategy in a “one-pot” synthetic method. In details, 2 mg MSDc and 2 mg NH2-PEG$_n$-SH (MW 2000 Da) were dissolved in 4 mL deionized water, following the addition of 1 mL 10 mM chloroauric acid solution. After 3-min magnetic stirring at 500 rpm, 5 mL 100 mM HEPES at pH 7.4 was added into the solution as the self-assembled catalyst. After 10-min stirring, the mixed liquor turned from a canary turbid liquid to a fuchsia clear solution, and had an obvious Tyndall effect, implying the successful preparation of MSDNc supraparticle colloids. This successful self-assembled construction was further proved by Fourier Transform Infrared (FT-IR) spectroscopy and ultraviolet absorption (UV–Vis) spectrum. The infrared spectra of MSDNc and ^{PEG}N which is the MSDc-free blank of control carrier

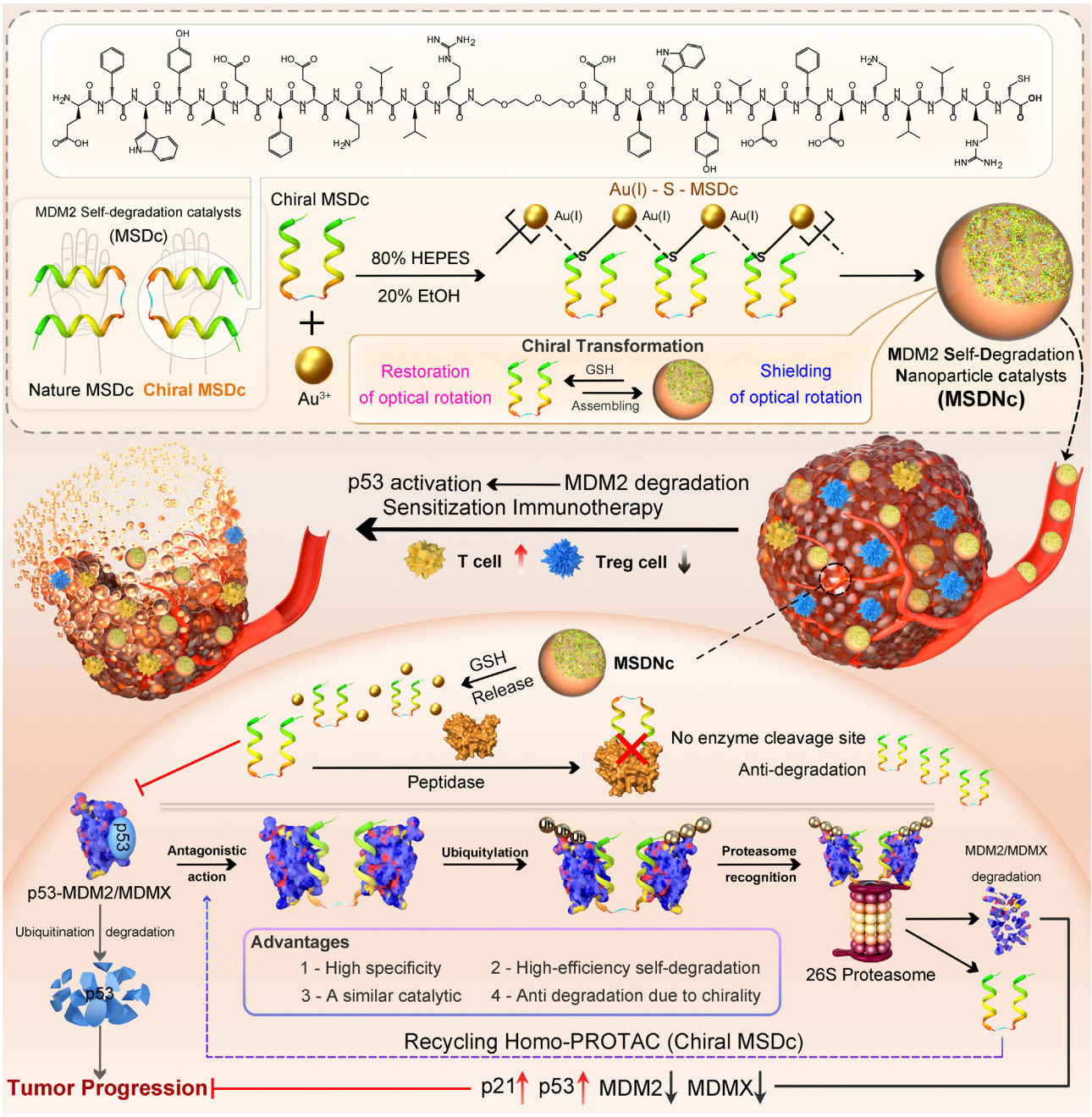

Fig. 1. The peptide-derived home-protac molecule MSDc, its nano-engineering strategy, and anti-tumor mechanism. The peptide is composed of two MDM2 affinity peptides, which can simultaneously bind to two MDM2 proteins and cause their subsequently mutual ubiquitination and degradation. The corresponding nano-engineered particle MSDNc relies on the self-assembly of $[Au(I)\text{-}S\text{-}MP]_n$. MSDNc reverses the p53 level in tumor tissues through the MDM2 degradation pathway, and synergistically enhances the anti-tumor effect of anti-pd1 immunotherapy.

showed differential absorption at 3250 cm^{-1} and 1650 cm^{-1}, which was caused by the amino and amide bonds [36] of MSDc in MSDNc (Fig. 2B&S1F). This result was proved again by the characteristic absorption peaks of peptides in UV–Vis spectrum at 280 nm (Fig. 2C&S1E), confirming the fabrication process of MSDNc which is consistent with our expectations. Moreover, Transmission electron microscope (TEM) images show that MSDNc is relatively uniform in size and exhibits good monodisperse characteristics (Fig. 2D). And dynamic light scattering (DLS) analysis confirmed that MSDNc had an average hydrodynamic diameter of 21.4 nm in a narrow peak distribution, further illustrating that MSDNc has good uniformity in size (Fig. 2E). In addition, we performed elemental analysis and diffraction analysis on MSDNc through a high-resolution transmission microscope. The superposition images of bright fields and various elements under the same view show that the gold, nitrogen, oxygen, and sulfur elements in MSDNc are uniformly distributed, which indicates the homogeneity of peptides and gold in the nanoparticles (Fig. 2F). Energy Dispersive X-Ray Spectroscopy (EDS) analysis shows that the elements of MSDNc are consistent with those of its reactants (Fig. 2G). Furthermore, as shown in Fig. S2, the size of diffraction fringe of MSDNc is slightly smaller than that of ^{PEG}N, suggesting the formation of gold-peptide supraparticle. Meanwhile, there is no significant difference of the lattice structure between MSDNc and ^{PEG}N, suggesting peptide has no obvious influence for the crystal structure (Figure S2).

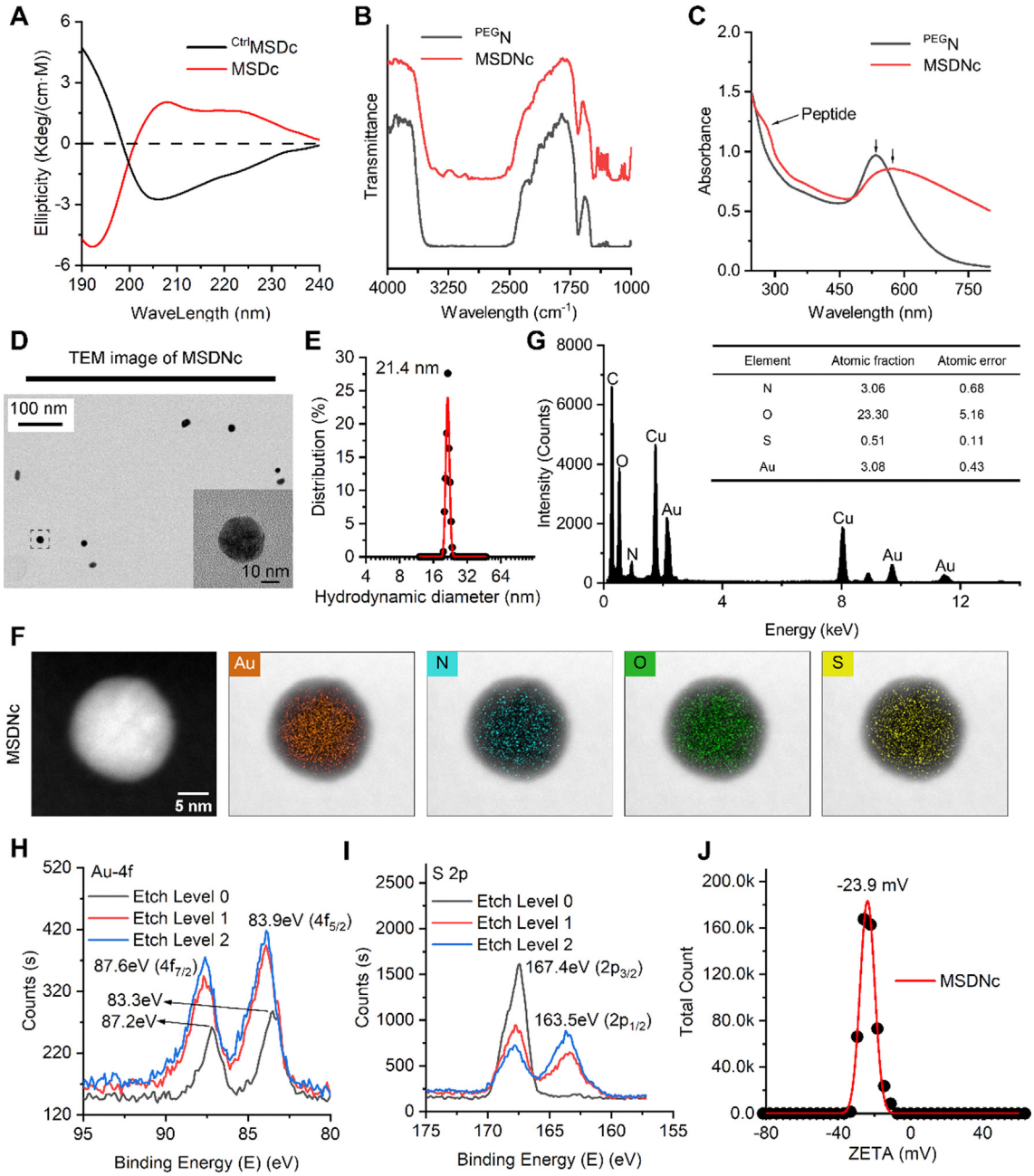

Fig. 2. Preparation and characterization of MSDNc. (A) Circular dichroism spectrum of MSDc (red line) and natural ^{Ctrl}MSDc (black line). The opposite absorption curve characterizes the chiral characteristics of MSDc. (B) FTIR spectra of MSDNc (red line) and ^{PEG}N (black line), Au-S bond absorption near 2950 cm^{-1} verify the formation process of MSDNc. (C) UV–Vis absorption spectra of MSDNc (red line) and ^{PEG}N (black line). The red shift of the absorption peak near 530 nm revealed the increase of nano size of MSDNc, compared with ^{PEG}N. (D) TEM image and partial magnification of MSDNc. (E) Hydrodynamic diameter distributions of MSDNc measured in PBS at pH 7.4. (F) The element analysis of Au, N, O, S overlay with a bright field image of MSDNc. (G) EDS analysis of MSDNc. (H&I) XPS spectra of Au 4f (H) and S 2p (I) at the surface and after etching of MSDNc. (J) Zeta potential of MSDNc measured in PBS at pH 7.4.

X-ray photoelectron spectroscopy (XPS) also shows that Au(I) is conjugated with the sulfhydryl group of MSDc. The XPS results of element Au 4f (Fig. 2H) show that the Au signal is smaller on the surface layer, and the signal is significantly enhanced after etching, and the peak position shifts in the positive direction. This indicates that the inner layer of Au^{1+} is mainly bound to the polypeptide through covalent bonds, while the outer layer of Au^{1+} can also be bound by coordination with the sulfhydryl group of the polypeptide. Similarly, the XPS results of S 2p (Fig. 2I) show that the sulfur in the outer layer of MSDNc exists mainly in the form of thiols, and as the etching depth increases, the free sulfhydryl signal decreases, which is consistent with the XPS results of Au [12,37,38]. Besides, MSDNc has a negative zeta potential with large absolute value (Fig. 2J), indicative of good colloidal stability that was further approved by the DLS analysis in the treatment of PBS buffer containing 20% fetal bovine serum (Figure S3).

MSDNc possessed favorable physicochemical and pharmaceutical properties

The diverse variety of protease and peptidase in the human body is a great threat to peptide therapeutics. To verify the effect of chirality on improving the proteolysis resistance, we treated chiral MSDc and natural ^{Ctrl}MSDc with chymotrypsin, and used high-

performance liquid chromatography (HPLC) to determine the content of the residual peptides [12,30]. As expected, L-enantiomeric ^{Ctrl}MSDc was completely degraded after the 12-hour treatment (Fig. 3A), while MSDc was hardly proteolyzed (the residual rate is 91.2%) (Fig. 3B). Further quantitative analysis revealed that the half-life of ^{Ctrl}MSDc against chymotrypsin was less than 0.3 h in sharp contrast to the MSDc with over 12-hour half-life (Fig. 3C).

In the synthesis process of MSDNc, the Au-S bond is crucial for the self-assembly of nanoparticles. The highly reducing environment in tumor cells (GSH concentration up to 10 mM) may reduce the Au-S bond and trigger the release of the peptide MSDc [12,38]. Incubating with 10 mM GSH for 6 h, the MSDNc solution became transparent, demonstrating the disassembly of MSDNc (Fig. 3D). This result was proved again by TEM image, in which MSDNc supraparticles were disappeared after GSH treatment. Next, the GSH-triggered cargo release was time-dependently monitored by HPLC. The 10 mM GSH incubation resulted in about 70% release within 3 h, whereas hardly any release can be found upon GSH-free incubation (Fig. 3E). Collective, these results demonstrated that MSDNc possessed favorable physicochemical and pharmaceutical properties including the proteolysis resistance, prolonged blood circulation, low immunogenicity and the GSH-triggered disassembly as well as the subsequent cargo release.

Another key design of MSDNc was the racemization, which is largely due to the flexibility of the gold-sulfur interface. Expectedly, this racemization of MSDNc was proved by CD spectrum, where nearly the whole ellipticity of MSDc was disappeared after the their self-assembly into MSDNc (Fig. 3F). Theoretically, this racemization can decrease the T-lymphocyte/macrophage phagocytose, which was approved by cellular uptakes test following the 6-h incubation with Cy3-labaled MSDc and MSDNc (Fig. 3G and S4). Besides, colloid stability is another critical factor for the circulation of nanomedicine. In order to verify the colloidal stability of MSDNc, solutions with different pH of 7.4, 6.5, 5.5, and 4.0, and containing 20% serum were prepared. DLS results show that under the above pH conditions, the size of MSDNc hardly changes within 12 h (Figure S3), suggesting the good colloidal stability in physiological environment and the subsequent escape from the reticuloendothelial system. Both the satisfactory T-lymphocyte/macrophage escape and the colloidal stability compelled us to investigated the blood circulation of MSDNc. Towards this end, the Cy3 fluorescence intensity in the blood was quantified after the intravenous injection of Cy3-labaled MSDc and MSDNc into healthy C57/B6 mice at the dosage of 1.5 mg/Kg. The fluorescence intensity of MSDNc is significantly higher than that of MSDc (Fig. 3H), indicative of the increased blood circulation after the supramolecular self-assembly.

In addition, the immune response triggered by the immunogenicity of foreign drugs, particularly non-anthropogenic chiral molecules, may bring huge side effects to the patient's treatment. Therefore, we used the enzyme linked immunosorbent assay (ELASA) to further analyze the immunogenicity indicators such as EPO, IL2, INF-γ, and EOS in the blood after administration (Fig. 3-I-L). Compared with the control group, the EPO content in the blood of the MSDc group decreased, and the levels of IL2, INF-γ and EOS were all significantly increased, indicating that the administration of the MSDc triggered a severe immune response in mice. The MSDNc group and the control group have no significant changes in immune indicators, indicating that MSDNc has almost no immunogenicity.

MSDNc degraded MDM2 and restored p53, thereby effectively killing tumor cells in vitro

MDM2 is a E3 Ubiquitin ligase and thus has the potential to be self-degraded by the homo- PROTAC, MSDc. As our design, the intracellular released MSDc can induce the homologous dimerization of MDM2, thereby promoting the self-degradation (Fig. 4A). Of note, due to the resistance against enzymatic hydrolysis, MSDc can cyclically catalyze this self-degradation reaction (Fig. 4A). The efficiency of MSDNc of inducing MDM2 degradation was evaluated by Western blotting in the human lung cancer cell line 1650, which carries wild-type p53 and overexpressed MDM2. After treating 1650 cells with 100 nM MSDNc for 48 h, the performed western blot image (Fig. 4B) and its quantified results (Fig. 4C) showed the down-regulated MDM2 level. In contrast, MSDc could not degraded intracellular MDM2 significantly (Figure S5), due to the poor ability of passive membrane penetration, the extensive clearance caused by macrophage and low bioavailability *in vivo* of peptide MSDc which have been proved by results of Fig. 3G&H. In order to further explore the mechanism of MSDNc degradation of MDM2, we pretreated the 1650 cell line with the proteasome inhibitor MG132 or the ubiquitinase inhibitors PYR-41, both of which interfered with the degradation efficacy of MSDNc (Fig. 4B&C). These results indicated that the degradation of MDM2 induced by MSDNc is mainly dependent on the degradation pathway of ubiquitination, which is consistent with our prediction.

For further validation of mechanism, proteomics analysis measured by triple quadrupole system was performed in the 1650 cells incubating with PBS (Control) or MSDNc for 12 h. The volcano graph in Fig. 4D showed 290 differential proteins including 183 up-regulated ones and 107 down-regulated ones. Furthermore, cluster analysis (Fig. 4E) and gene set enrichment analysis (GSEA) (Fig. 4F) of the p53 signaling pathway indicated the activated p53 signaling pathway in response to MSDNc treatment. Meanwhile, we conducted GSEA on other pathways related to p53, and found five signal pathways with significant enrichment of differential genes: p53 downstream pathway (Figure S6), apoptosis (Fig. 4G), cell cycle (Fig. 4H), cell cycle checkpoints (Fig. 4I), and cell cycle mitotic (Fig. 4J). These results showed that MSDNc significantly up-regulated p53 signaling pathways, and induced apoptosis and cycle arrest of cancer cells. Moreover, the image and quantized data of western blot (Fig. 4K and S7) and immunofluorescence (Fig. 4L and 4 M) proved again the restoration of p53 signaling pathways by MSDNc. Additionally, these results also showed MSDNc possessed increased action than its L-enantiomer ^{Ctrl}MSDNc in activating p53 signaling pathways, suggesting the superiority of chiral supramolecules. In line with the above results, MSDNc showed the potent inhibition action of cancer cell viability (Fig. 4N) and the increased inducibility cell cycle arrest as well as apoptosis (Fig. 4O&P, Figure S8) in more action than ^{Ctrl}MSDNc. Moreover, similar results were also observed in A549 (Figure S9), LLC (Figure S10) and B16F10 cell lines (Figure S11). Collectively, these results demonstrated that MSDNc potently degraded MDM2 and restored p53 in more action than ^{Ctrl}MSDNc, thereby presenting intensive anti-cancer action.

MSDNc potently suppressed tumor growth in vivo through p53 restoration

Tumor targeting ability plays important role in the anti-cancer action of nanomedicine, and contribute directly to the off-target toxicity and biological safety [32,33,39]. The enhanced penetration and retention effect (EPR) of tumor vascular tissue is an important basis for the passive targeting of nanoparticles to tumor sites [40–42]. To explore the biodistribution, a allograft model of melanoma was established by subcutaneously inoculating 5×10^5 Bl6F10 cells into the haunch of immune-sound C57/B6 mice [43]. MSDNc was injected intravenously into tumor-bearing mice, and the inductively coupled plasma mass (ICP-Mass) was used to detect ^{197}Au in various organs at different time points. As shown in Fig. 5A, MSDNc showed satisfactory tumor enrichment. Moreover,

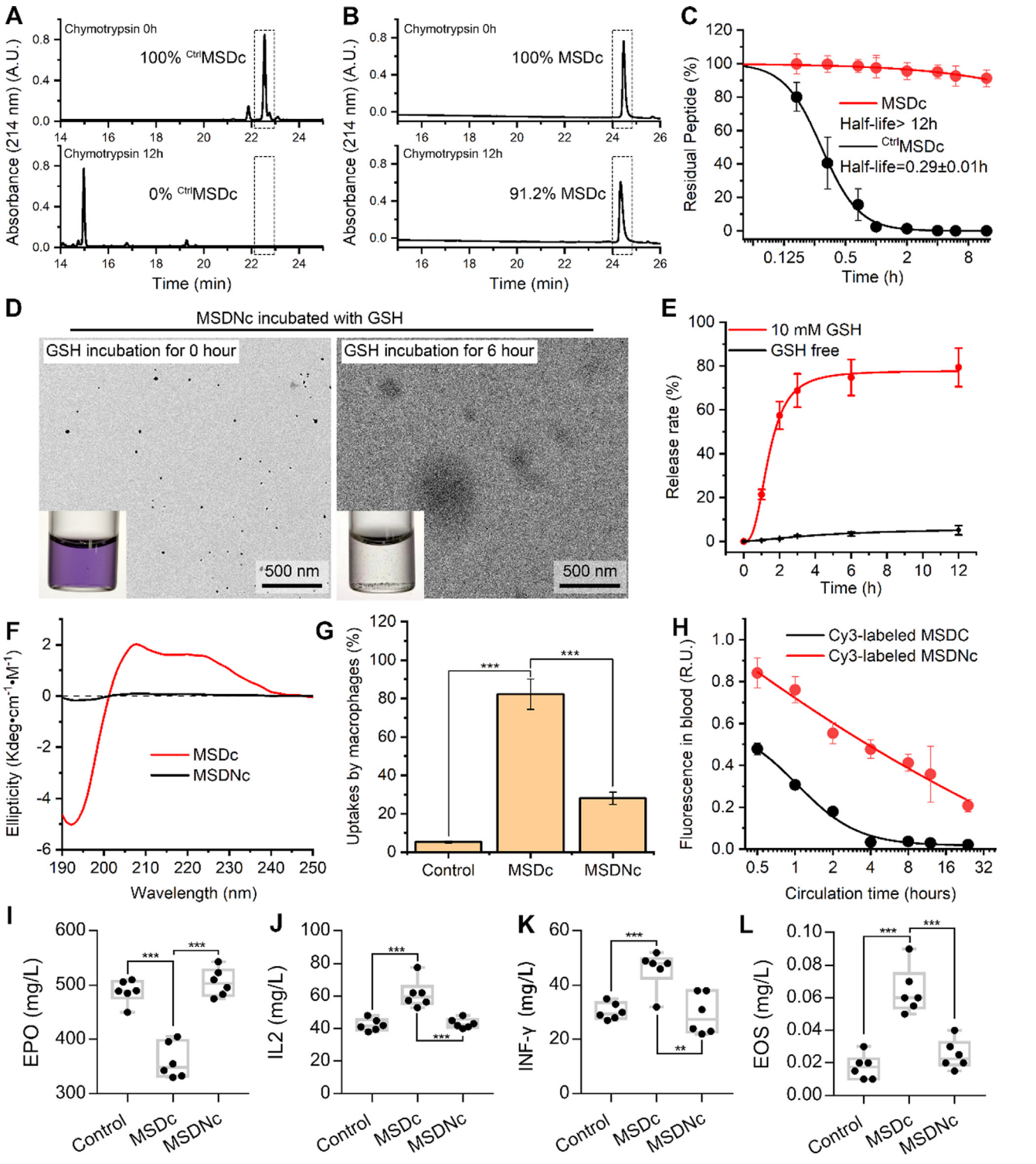

Fig. 3. MSDNc with a good proteolytic resistance, biological stability, GSH-responsive cargo release. (A&B) Residual peptide of L ^{Ctrl}MSDc (A) and MSDc (B) in PBS treated by 0.5 mg/ml chymotrypsin for 12 h measured by HPLC. (C) Proteolysis resistance of MSDc (red) and ^{Ctrl}MSDc (black) under PBS containing 0.5 mg/ml chymotrypsin. (D) TEM images of untreated MSDNc (left) and MSDNc treated with 10 mM GSH for 6 h (right). (E) Cargo release rate of MSDNc over time without no treatment (black) or after treated with 10 mM GSH (red) measured by HPLC. (F) Circular dichroism spectrum of MSDc (red line) and MSDNc (black line). (G) After treating cells with a drug concentration of 1 μM for 6 h, the uptake efficiency of FITC-labeled MSDNc and FITC-labeled MSDc by macrophages analysed by flow cytometry. (H) The fluorescence in bood of Cy3-labeled MSDc (black) and MSDNc (red) after tail vein injection at a dose of 1.5 mg/kg. (I-L) The content of EPO (I), IL2 (J), INF (K), and EOS (L) in the blood measured by ELASA after the above-mentioned administration.

a time-dependent tendency for tumor accumulation can be found through the further analyzed the ration of MSDNc in tumors to other organs (Fig. 5B). For the investigation of the *in vivo* anti-cancer action, 20 mice bearing tumors with the volume about 100 mm^3 were randomly divided into four groups (n = 5/group), and intravenously administered with normal saline (Control), ^{PEG}-N, ^{Ctrl}MSDNc and MSDNc at a dose of 2 mg/kg every other day for four times. After 9-day treatments, all mice were sacrificed and

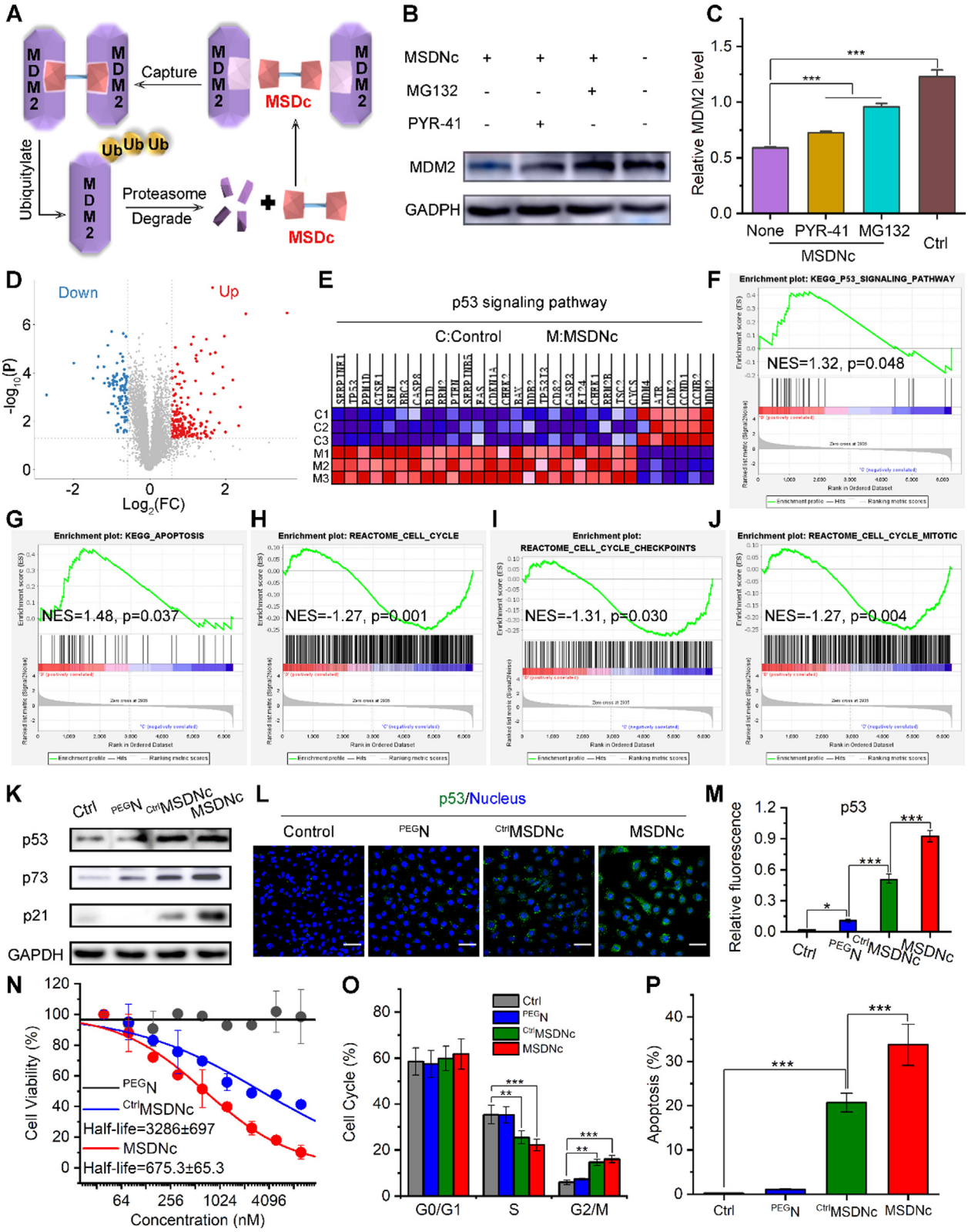

Fig. 4. MSDNc degrades MDM2 and restores p53 levels, thereby effectively killing tumor cells *in vitro*. (A) Schematic diagram of degradation of MDM2 by MSDNc through home-protac mechanism. (B&C) After 1650 cells were pretreated with MG132 or PYR-41 for 12 h, and incubated with MSDNc at a dose of 100 nm for 48 h, western blot was performed (B) and the relative MDM2 level were quantified (C) to analyze the expression of MDM2 proteins, and GAPDH was used as an internal reference protein. (D) After MSDNc treatment, the volcano plot of the differential changes in gene expression in 1650 cell line was shown. The absolute value of the base 2 logarithm of the genetic difference is required to be>1.3, and the adjusted p value should be>0.05. (E&F) GSEA result (E) and hierarchical clustering of genes (F) for p53 signaling pathway. (G-J) GSEA results for KEGG apoptosis, REACTOME cell cycle, REACTOME cell cycle checkpoints and REACTOME cell cycle mitotic. (K) After 1650 cells were treated by ^{PEG}N, ^{Ctrl}MSDNc, and MSDNc at a dose of 100 nm for 48 h, and then western blot was performed to analyze the expression of p53, p73 and p21 proteins, and GAPDH was used as an internal reference protein. (L&M) Immunofluorescence staining (L) and quantitative analysis (M) of p53 were performed in the 1650 cell line after above treatment. (N) The cell viability was measured by MTT after treated by ^{PEG}N, ^{Ctrl}MSDNc and MSDNc at different concentration in 1650 cell line. (O&P) The cell cycle (O) and apoptosis (P) were analysed by flow cytometry after treated by ^{PEG}N, ^{Ctrl}MSDNc and MSDNc at a dose of 100 nm for 48 h.

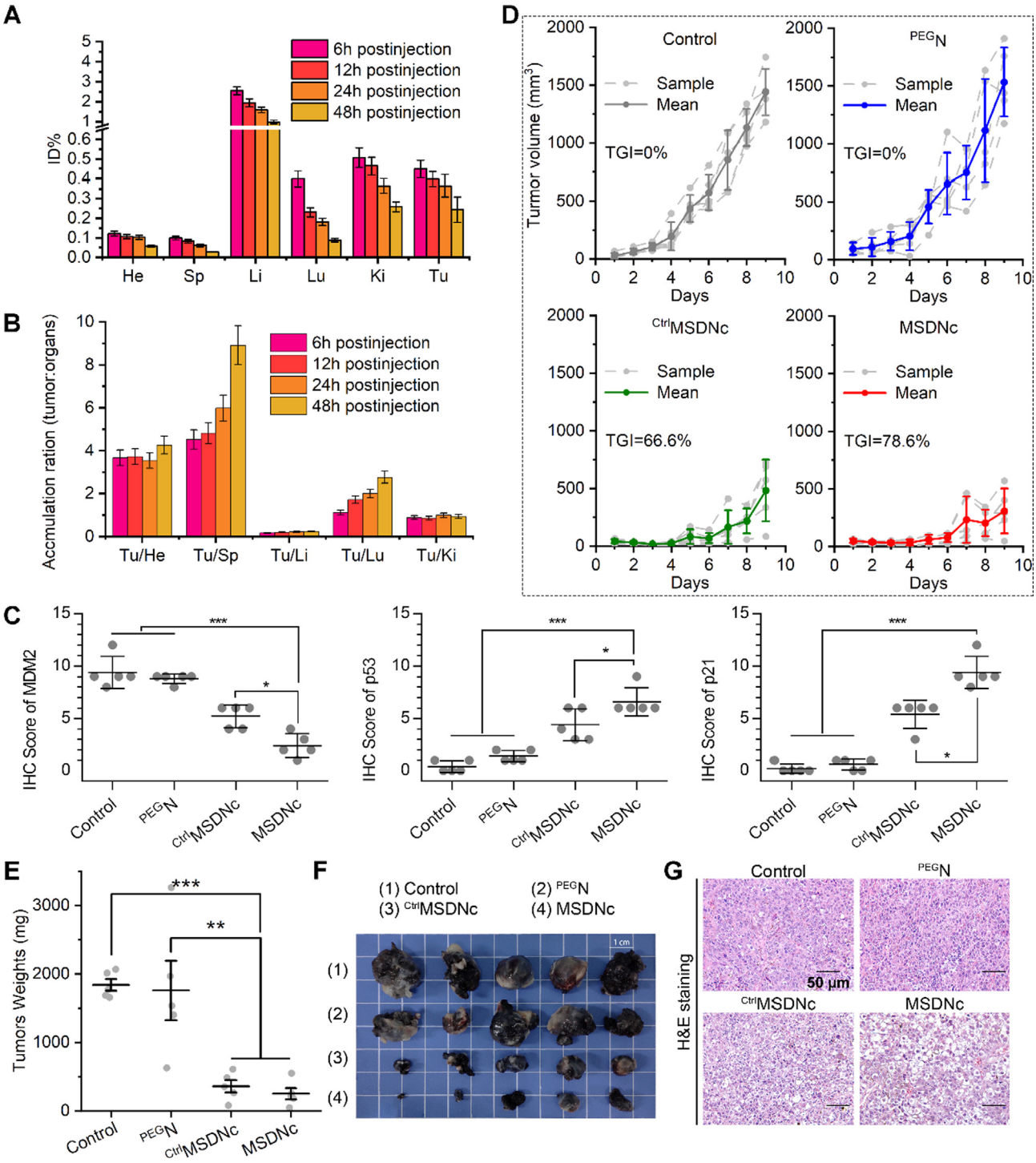

Fig. 5. MSDNc has good targeting ability *in vivo*, effectively restores p53 levels, and inhibits tumor proliferation. The melanoma subcutaneous allograft c57 model was established (every mouse was injected with 5×10^5 B1610 cells subcutaneously.). (A) Drug metabolism of MSDNc. Gold concentration in several tissues, including heart, spleen, liver, lung, kidney, and tumor were measured at 6 h, 12 h, 24 h, 48 h after dosing by ICP-MS. (B) tumor: organ ratios of MSDNc at the above several time points. The data were shown as mean ± SD. After inoculation with tumor cells, the mice were randomly divided into four groups (n = 5/group). Normal saline, ^{PEG}N, ^{Ctrl}MSDNc, MSDNc were intravenously injected at a dose of 2 mg/kg at day 1, 3, 5, and 7. And all the mice were sacrificed at day 9. (C) The quantify scores of immunohistochemical staining images of MDM2, p53 and p21 were performed in dissected tumor tissues. (D) Tumor growth curves of each group in c57 mice during the treatment cycle. (E) Tumor weights of c57 mice in each group after treatment. (F) Tumor images of each group after treatment. (G) H&E staining images of tumor tissues dissected of each group.

their tumor tissues were dissected. The immunohistochemical staining on the isolated tumor tissues was performed to explore the ability of MSDNc to degrade MDM2 and restore p53 *in vivo* (Figure S11). As shown in Fig. 5C, the score of images of immunohistochemistry demonstrated that MSDNc has achieved better performance than ^{Ctrl}MSDNc in down-regulating MDM2 and activating p53. In line with it, MSDNc also significantly restored the levels of the p53 downstream signaling molecule p21 (Fig. 5C). After the administration, ^{Ctrl}MSDNc and MSDNc showed tumor growth inhibition (TGI) rates of 66.6% and 78.6% in comparison with control, whereas ^{PEG}N showed hardly any inhibition efficiency (Fig. 5D), suggesting that all inhibitory effect attributed to

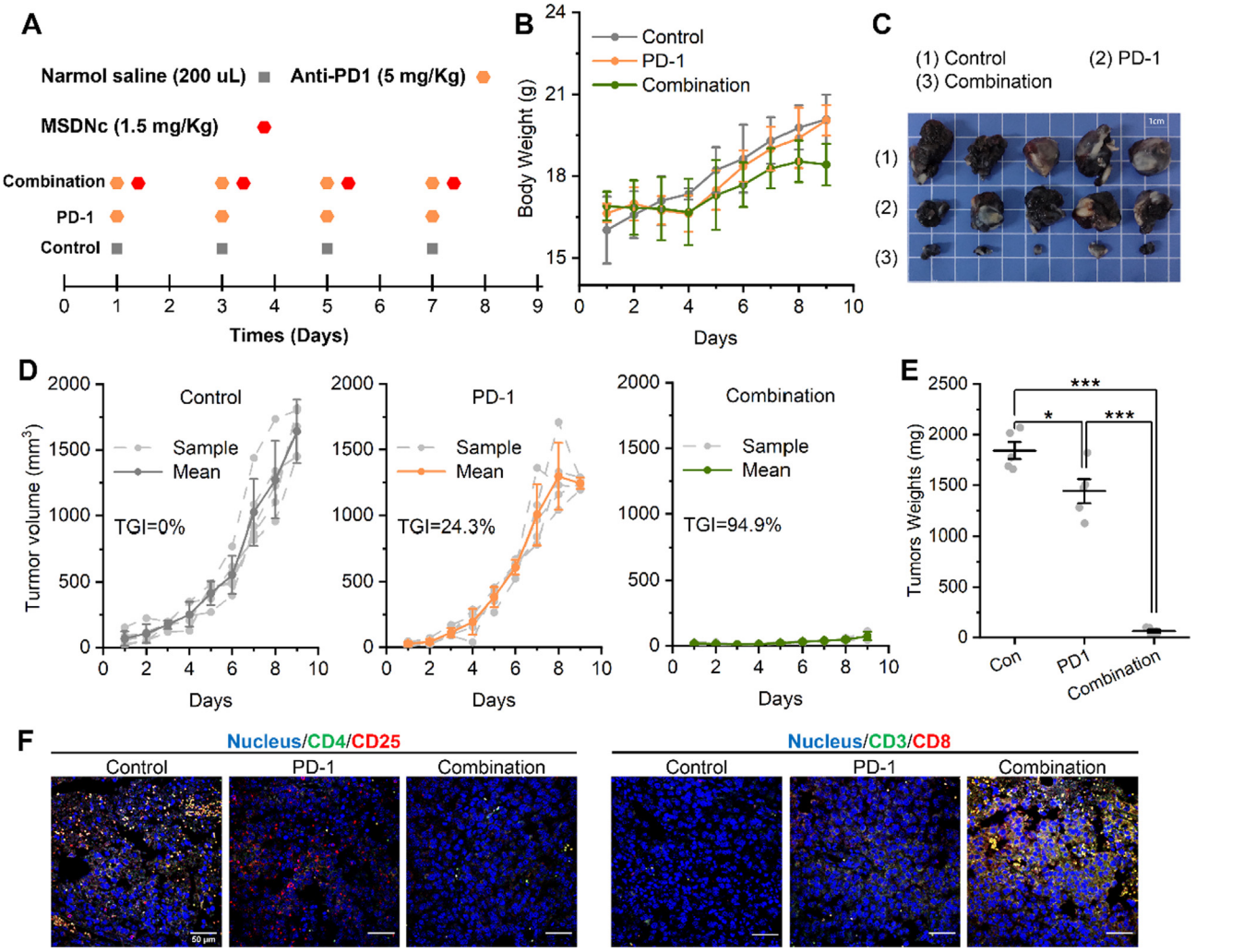

Fig. 6. MSDNc activates CD8⁺ T cells and sensitizes PD-1 therapy. (A) Administration schedule of normal saline, anti-PD1, and combination. (B) Body weights of mice in each group during treatment. (C) Tumor images after treatment. (D) Tumor growth curves after treatment. (E) Tumor weights of c57 mice after treatment. (F) Immunofluorescence staining of CD4/CD25 and CD3/CD8 of dissected tumor tissues in each group.

peptide cargo other than carrier. The dissected tumor weight and tumor photos also confirmed the powerful tumor suppression effect of MSDNc in more action than ^{Ctrl}MSDNc (Fig. 5E&F). Of note, as shown in Fig. 5F, two tumors in MSDNc-treated group almost disappeared, which further illustrated the extreme potency of MSDNc. These results were approved again by the hematoxylin-eosin (HE) staining of tumor sections (Fig. 5G). These results collectively indicated that MSDNc had a strong tumor suppressor effect *in vivo* by inducing the degradation of MDM2 and subsequent recovery of p53.

MSDNc activated CD8⁺ T cells and sensitized PD-1 therapy

In order to further explore the application potential of MSDNc in anti-tumor immunotherapy, we studied the synergistic effect of MSDNc and Anti-PD1 therapy in this allograft model of melanoma. 15 mice bearing tumors with the volume about 100 mm^3 were randomly divided into three groups (n = 5/group), and intravenously administered as the injection scheme in Fig. 6A. And the frequency of administration was consistent between the experimental group and the control group, which was once every two days. Notably, the dosage of MSDNc was 2 mg/kg, and the one of Anti-PD1 (murine monoclonal antibody) was 5 mg/kg. During the 9-day treatment, no statistically significant change can be found among the three group (Fig. 6B), suggesting the therapeutic safety. After 9-day administration, the combined treatment presented an inhibitory rate of 94.9% on melanoma in sharp contrast to the monotherapy by Anti-PD1 (Fig. 6C). Images of isolated mouse tumor tissue and tumor weight also showed similar results (Fig. 6D&E). Immunofluorescence staining of tumor tissues showed that compared with the control group and anti-PD-1 antibody group, the combined treatment significantly increased the number of cytotoxic T lymphocytes (CD3⁺/CD8⁺ T cells) and significantly reduced the regulatory ability of T lymphocytes (CD4⁺/CD25⁺ T cells) in tumor tissues (Fig. 6F). These results indicated that the MSDNc activated CD8 + T cells and sensitized PD-1 therapy.

MSDNc maintained good biological safety

Nowadays, metabolizable and scrapable nanotherapeutics showed reduced toxicity, presumably because of the elimination of the unwanted accumulation [42,44,45]. As our design, triggered by intracellular GSH, MSDNc disassembled into ultra-small nanoparticles, which may be efficiently removed from human body. To verify it, MSDNc was injected intravenously into healthy C57/B6 mice, and ICP-Mass was used to detect ^{197}Au in various organs at 2 h, 6 h, 12 h, 24 h, 48 h, 72 h and one week. ICP-Mass results (Fig. 7A) showed that the metabolism of MSDNc mainly

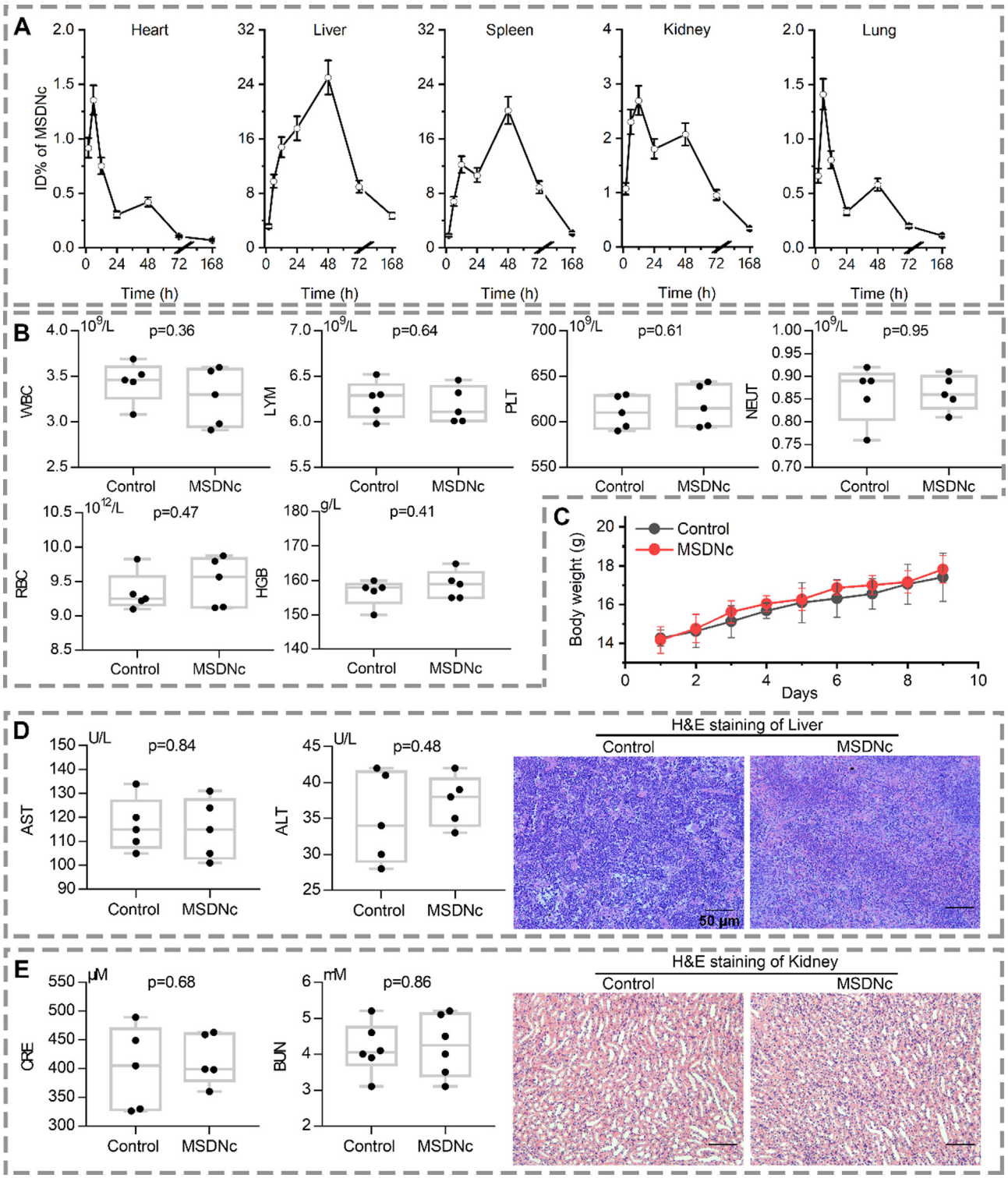

Fig. 7. MSDNc maintains good biological safety. (A) Organ distribution of MSDNc after drug was injected intravenously in healthy mice at a dose of 2 mg/kg. Gold concentration in several tissues, including heart, liver, spleen, lung, kidney was measured at 2 h, 6 h, 12 h, 24 h, 48 h, 3 days, 7 days by ICP-MS. The data were shown as mean ± SD. (B) Blood routine index was measured after the 9-day treatment. (Inject 200ul normal saline (Control group) or MSDNc intravenously every other day for 5 times). (C) Body weights of mice after above treatment. (D&E) The liver (D) and kidney (E) function were measured after the above administration, and corresponding H&E staining images is shown, respectively.

depends on the liver and kidneys, suggesting that MSDNc is mainly excreted from the body in the form of a mononuclear phagocytic system. Moreover, after a week, nearly all MSDNc in all organs was almost eliminated, which indicated that MSDNc is metabolizable and scrapable.

Next, we conducted a comprehensive toxicity study using normal and active C57/B6 mice. The mice were randomly divided into 2 groups, and were administered with saline or MSDNc through intravenous injection. The mice were intervened at a dose of 10 mg/kg every other day. After 5 dosing cycles, the blood routine

indexes of the mice were checked. In blood routine examination, there were also no significant differences in the levels of platelets, white blood cells, and lymphocytes among the two groups (Fig. 7B). The wight of mice in MSDNc group didn't show any abnormalities, compared with the control group (Fig. 7C). Since the liver and kidneys undertake most of the metabolic tasks of MSDNc, it is necessary to study the liver and nephrotoxicity caused by long term accumulation of MSDNc in the body. After 5 dosing cycles, the liver function (Fig. 7D) and renal function (Fig. 7E) of the mice was checked. As expected, the liver and kidney function indexes such as glutamate oxalate transaminase, glutamate-pyruvate transaminase, creatinine and blood urea nitrogen in the intervention group were not significantly different from those in the control group, and they were all within the normal physiological range (Fig. 7D&E). Besides, no obvious toxicity was found in pathological sections of the heart, liver, spleen, lung, and kidney (Fig. 7D&E, Figure S12). In summary, the above results indicated that MSDNc possessed good biological safety.

Discussion

The network of protein–protein interactions (PPIs) is the basis of vital activities in cells and between cells [46], and thus abnormal changes in this network would disrupt normal physiological activities of cells, causing diseases including cancer [47]. In consequence, regulating abnormal PPIs has huge potential for disease therapy, and many PPIs-targeting small molecules derived from natural compounds or pure organic synthesis have been developed [11]. Nevertheless, the vast majority of PPIs possess the smooth and flat contact interface, which cannot be targeted by small molecules with the limited affinity [11]. Fortunately, in recent years, the emerging Proteolysis-Targeting Chimeras (PROTAC) technology offered a high-efficiency method to solve this problem and substoichiometrically catalytically redress the anomalously up-regulated PPIs, by which E3 ubiquitin ligase can connect the target protein, thereby resulting in its ubiquitin-dependent degradation [48,49]. However, the development of PROTACs is often limited by the lack of small-molecular ligands for E3 ubiquitin ligase and the target protein [50]. Although many peptide fragments have been approved to be capable of binding E3 ligase and target protein with high affinity and consequently expanded the universality as well as practicality of PROTACs [50], clinical translation of PPIs-targeting peptides and peptide-derived PROTACs has been hampered by their instability against proteolysis, inefficacious cellular internalization and insufficient blood circulation [39,51]. In present work, these intrinsic pharmaceutical obstacles of peptides can be overcame well by D-enantiomerization and supramolecular construction, so we can say that the peptide-derived chiral supramolecular self-assembly strategy reported here provided a viable way to target PPIs, particularly these inside the cell.

As a well-known tumor suppressor, p53 protein can regulate the expression of a variety of target genes in response to DNA damage and oncogene activation [52]. Although p53 retains wild-type status in at least 50% of human tumors, its anti-cancer action and intracellular stability are abrogated by its negative regulatory molecule, an E3 ubiquitin ligase termed MDM2 [24,53]. A growing number of studies showed that the active restoration of endogenous p53 suppressed tumor progression through including apoptosis, cycle arrest and innate immune responses [54]. In addition, recent studies have pointed out the emerging role of p53 in anti-tumor immunity that p53 can directly activate the key regulators of immune signaling pathways such as IFN and TLR3, etc. [55]. Thus, antagonists or degradant of MDM2 that restore the p53 signaling pathway can potentially be developed into a class of therapeutics for anti-cancer therapy. Moreover, MDM2 can be triggered to self-degrade by homo-PROTACs as it is an E3 ubiquitin enzyme [56]. Thus, in this work, an identical chiral MDM2 affinity peptide [10,29–31] was dimerized by a triethylene glycol linker as a sub-stoichiometric MDM2 self-degradation catalyst (MSDc). After self-assembly into a racemic supraparticle termed MSDNc, this catalyst resulted in the potently homo-degradation of MDM2 *in vitro* and *in vivo*, thereby suppressing the tumor progression and synergizing the tumor immunotherapy in allograft model of melanoma through p53 restoration.

Conclusion

In this work, to design peptide-derived chiral supramolecular nanomedicine with suitable pharmaceutical properties for clinical translation, a mild and simple self-assembly strategy was developed to turn the building block - chiral peptide- into a spherical supraparticle exploiting a metal coordination between mercaptan in peptides and trivalent gold ion. Because of the flexibility of the gold-sulfur interface, this chiral gold spherical supraparticle undergone racemization, which eliminated the consume from the T-lymphocyte/macrophage phagocytose in circulation of D-enantiomeric peptides. In this proof-of-concept study, we design a D-peptide as MDM2 Self-Degradation catalysts (MSDc) to induce the self-degradation of a carcinogenic E3 Ubiquitin ligase termed MDM2 through the chemically linked dimerization of a MDM2 binding D-peptide. Self-assembling MSDc into a spherical supraparticle termed MDM2 Self-Degradation Nanocatalysts (MSDNc) resulted in the potently homo-degradation of MDM2. To further revealed the physiological and biochemical role of this supramolecular chirality *in vivo* and *in vitro*, the L-enantiomer of MSDc (^{Ctrl}MSDc) with the same capacity to catalyze MDM2 homo-degradation was designed and self-assembled into ^{Ctrl}-MSDNc for comparative study to MSDNc. As expected, MSDNc down-regulated MDM2 in more action than ^{Ctrl}MSDNc. More importantly, MSDNc preponderantly suppressed the tumor progression and synergized the tumor immunotherapy in allograft model of melanoma through p53 restoration in comparison to ^{Ctrl}-MSDNc. As it were, our work not only developed a secure and efficient therapeutic agent targeting MDM2 with the potential of clinical translation, but also provided a feasible and biocompatible strategy for the construction of peptide supraparticle and expanded the application of chiral therapeutic and homo-PROTAC to peptide-derived chiral supramolecular nanomedicine.

CRediT authorship contribution statement

Wenguang Yang: Methodology, Software, Visualization, Investigation. **Wenjia Liu:** Conceptualization. **Xiang Li:** Data curation, Investigation. **Jin Yan:** Writing – review & editing. **Wangxiao He:** Supervision, Writing – review & editing.

Declaration of Competing Interest

The authors declare that they have no known competing financial interests or personal relationships that could have appeared to influence the work reported in this paper.

Acknowledgements

This work was supported by National Natural Science Foundation of China (No. 32171256 for W. He, No. 22007076 for J. Yan and No. 81970915 for W. Liu), "The Young Talent Support Plan" of Xi'an Jiaotong University (For W. Liu and W. He), Thousand Talents Plan of Shaanxi Province (For W. He). We thank Instrument Analysis Center of Xi'an Jiaotong University for their assistance

with TEM, DLS, FT-IR and XPS analysis. We also appreciate the help of RNA-seq analysis from BioNovoGene (Suzhou) Co., Ltd.

Appendix A. Supplementary material

Supplementary data to this article can be found online at https://doi.org/10.1016/j.jare.2022.05.009.

References

[1] Milton FP, Govan J, Mukhina MV, Gun'ko YK. The chiral nano-world: chiroptically active quantum nanostructures. Nanoscale Horiz 2016;1(1):14–26. doi: https://doi.org/10.1039/c5nh00072f.

[2] Brandt JR, Salerno F, Fuchter MJ. The added value of small-molecule chirality in technological applications. Nat Rev Chem 2017;1(6):0045. doi: https://doi.org/10.1038/s41570-017-0045.

[3] Hein JE, Blackmond DG. On the Origin of Single Chirality of Amino Acids and Sugars in Biogenesis. Acc Chem Res 2012;45(12):2045–54. doi: https://doi.org/10.1021/ar200316n.

[4] Kumar A, Capua E, Kesharwani MK, Martin JML, Sitbon E, Waldeck DH, et al. Chirality-induced spin polarization places symmetry constraints on biomolecular interactions. Proc Natl Acad Sci U S A 2017;114(10):2474–8. doi: https://doi.org/10.1073/pnas.1611467114.

[5] Yeom J, Guimaraes PPG, Ahn HM, Jung B-K, Hu Q, McHugh K, et al. Chiral Supraparticles for Controllable Nanomedicine. Adv Mater 2020;32(1):1903878. doi: https://doi.org/10.1002/adma.v32.110.1002/adma.201903878.

[6] Basak S, Singh I, Ferranco A, Syed J, Kraatz HB. On the Role of Chirality in Guiding the Self-Assembly of Peptides. Angew Chem Int Ed 2017;56(43):13288–92. doi: https://doi.org/10.1002/anie.201706162.

[7] Zhou Q, Yu L-S, Zeng S. Stereoselectivity of chiral drug transport: a focus on enantiomer–transporter interaction. Drug Metab Rev 2014;46(3):283–90. doi: https://doi.org/10.3109/03602532.2014.887094.

[8] Nguyen LA, He H, Pham-Huy C. Chiral drugs: an overview. Int J Biomed Sci 2006;2(2):85–100.

[9] Agranat I, Caner H, Caldwell J. Putting chirality to work: the strategy of chiral switches. Nat Rev Drug Discov 2002;1(10):753–68. doi: https://doi.org/10.1038/nrd915.

[10] Yan J, Yao Yu, Yan S, Gao R, Lu W, He W. Chiral protein supraparticles for tumor suppression and synergistic immunotherapy: An enabling strategy for bioactive supramolecular chirality construction. Nano Lett 2020;20(8):5844–52. doi: https://doi.org/10.1021/acs.nanolett.0c0175710.1021/acs.nanolett.0c01757.s001.

[11] Nevola L, Giralt E. Modulating protein-protein interactions: the potential of peptides. Chem Commun 2015;51(16):3302–15. doi: https://doi.org/10.1039/c4cc08565e.

[12] Yan J, Ji F, Yan S, You W, Ma F, Li F, et al. A general-purpose Nanohybrid fabricated by Polymeric Au(I)-peptide precursor to wake the function of Peptide Therapeutics. Theranostics 2020;10(19):8513–27. doi: https://doi.org/10.7150/thno.47243.

[13] He W, Yan J, Jiang W, Li S, Qu Y, Niu F, et al. Peptide-induced self-assembly of therapeutics into a well-defined nanoshell with tumor-triggered shape and charge switch. Chem Mater 2018;30(20):7034–46. doi: https://doi.org/10.1021/acs.chemmater.8b02572.

[14] Bian Z, Yan J, Wang S, Li Y, Guo Yi, Ma B, et al. Awakening p53 in vivo by D-peptides-functionalized ultra-small nanoparticles: Overcoming biological barriers to D-peptide drug delivery. Theranostics 2018;8(19):5320–35. doi: https://doi.org/10.7150/thno.27165.

[15] Luo Z, Zhang S. Designer nanomaterials using chiral self-assembling peptide systems and their emerging benefit for society. Chem Soc Rev 2012;41(13):4736–54. doi: https://doi.org/10.1039/c2cs15360b.

[16] Zhou J, Kroll AV, Holay M, Fang RH, Zhang L. Biomimetic Nanotechnology toward Personalized Vaccines. Adv Mater 2020;32(13):1901255. doi: https://doi.org/10.1002/adma.v32.1310.1002/adma.201901255.

[17] Zhang S. Fabrication of novel biomaterials through molecular self-assembly. Nat Biotechnol 2003;21(10):1171–8. doi: https://doi.org/10.1038/nbt874.

[18] Green DW, Lee J-M, Kim E-J, Lee D-J, Jung H-S. Chiral Biomaterials: From Molecular Design to Regenerative Medicine. Adv Mater Interfaces 2016;3(6):1500411. doi: https://doi.org/10.1002/admi.201500411.

[19] Wade D, Boman A, Wåhlin B, Drain CM, Andreu D, Boman HG, et al. All-D amino acid-containing channel-forming antibiotic peptides. Proc Natl Acad Sci U S A 1990;87(12):4761–5. doi: https://doi.org/10.1073/pnas.87.12.4761.

[20] Cecconello A, Besteiro LV, Govorov AO, Willner I. Chiroplasmonic DNA-based nanostructures. Nat Rev Mater 2017;2(9):17039. doi: https://doi.org/10.1038/natrevmats.2017.39.

[21] Park JI, Nguyen TD, de Queirós Silveira G, Bahng JH, Srivastava S, Zhao G, et al. Terminal supraparticle assemblies from similarly charged protein molecules and nanoparticles. Nat Commun 2014;5(1). doi: https://doi.org/10.1038/ncomms4593.

[22] Piccinini E, Pallarola D, Battaglini F, Azzaroni O. Self-limited self-assembly of nanoparticles into supraparticles: towards supramolecular colloidal materials by design. Mol Syst Des Eng 2016;1(2):155–62. doi: https://doi.org/10.1039/C6ME00016A.

[23] Xia Y, Nguyen TD, Yang M, Lee B, Santos A, Podsiadlo P, et al. Self-assembly of self-limiting monodisperse supraparticles from polydisperse nanoparticles. Nat Nanotechnol 2011;6(9):580–7. doi: https://doi.org/10.1038/nnano.2011.121.

[24] Wade M, Li Y-C, Wahl GM. MDM2, MDMX and p53 in oncogenesis and cancer therapy. Nat Rev Cancer 2013;13(2):83–96. doi: https://doi.org/10.1038/nrc3430.

[25] Yang G, Zhang J, Yan J, You W, Hou P, He W, et al. Modulating protein–protein interactions in vivo via peptide-lanthanide-ferived nanoparticles for hazard-free cancer therapy. J Biomed Nanotechnol 2019;15(9):1937–47. doi: https://doi.org/10.1166/jbn.2019.2820.

[26] Niu F, Yan J, Ma B, Li S, Shao Y, He P, et al. Lanthanide-doped nanoparticles conjugated with an anti-CD33 antibody and a p53-activating peptide for acute myeloid leukemia therapy. Biomaterials 2018;167:132–42.

[27] Ma B, Niu F, Qu X, He W, Feng C, Wang S, et al. A tetrameric protein scaffold as a nano-carrier of antitumor peptides for cancer therapy. Biomaterials 2019;204:1–12.

[28] He S, Ma J, Fang Y, Liu Y, Wu S, Dong G, et al. Homo-PROTAC mediated suicide of MDM2 to treat non-small cell lung cancer. Acta Pharmaceutica Sinica B 2021;11(6):1617–28.

[29] Yan J, Yan S, Hou P, Lu W, Ma PX, He W, et al. A Hierarchical Peptide-Lanthanide Framework To Accurately Redress Intracellular Carcinogenic Protein-Protein Interaction. Nano Lett 2019;19(11):7918–26. doi: https://doi.org/10.1021/acs.nanolett.9b03028.

[30] He W, Yan J, Sui F, Wang S, Su Xi, Qu Y, et al. Turning a Luffa protein into a self-assembled biodegradable nanoplatform for multitargeted cancer therapy. ACS Nano 2018;12(11):11664–77. doi: https://doi.org/10.1021/acsnano.8b07079.

[31] Yan J, He W, Yan S, Niu F, Liu T, Ma B, et al. Self-assembled peptide-lanthanide nanoclusters for safe tumor therapy: overcoming and utilizing biological barriers to peptide drug delivery. ACS Nano 2018;12(2):2017–26. doi: https://doi.org/10.1021/acsnano.8b00081.

[32] Yan J, He W, Li X, You W, Liu X, Lin S, et al. Carnosic acid-induced co-self-assembly of metal-peptide complexes into a nanocluster-based framework with tumor-specific accumulation for augmented immunotherapy. Chem Eng J 2021;416:129141. doi: https://doi.org/10.1016/j.cej.2021.129141.

[33] Liu T, Yan J, He C, You W, Ma F, Chang Z, et al. A tumor-targeting metal-organic nanoparticle constructed by dynamic combinatorial chemistry toward accurately redressing carcinogenic Wnt cascade. Small 2022;18(3):2104849. doi: https://doi.org/10.1002/smll.202104849.

[34] Yang G, Zhang J, You W, Zhao X, Hou P, He W, et al. Targeted disruption of the BCL9/β-catenin interaction by endosomal-escapable nanoparticles functionalized with an E-cadherin-derived peptide. Nanotechnology 2020;31(11):115102. doi: https://doi.org/10.1088/1361-6528/ab5a03.

[35] He W, Mazzuca P, Yuan W, Varney K, Bugatti A, Cagnotto A, et al. Identification of amino acid residues critical for the B cell growth-promoting activity of HIV-1 matrix protein p17 variants. BBA-Gen Subjects 2019;1863(1):13–24. doi: https://doi.org/10.1016/j.bbagen.2018.09.016.

[36] Zheng X, Yan J, You W, Li F, Diao J, He W, et al. De novo nano-erythrocyte structurally braced by biomimetic Au(I)-peptide skeleton for MDM2/MDMX predation toward augmented pulmonary adenocarcinoma immunotherapy. Small 2021;17(20):. doi: https://doi.org/10.1002/smll.202100394e2100394.

[37] Yan S, Yan J, Liu D, Li X, Kang Q, You W, et al. A nano-predator of pathological MDMX construct by clearable supramolecular gold(I)-thiol-peptide complexes achieves safe and potent anti-tumor activity. Theranostics 2021;11(14):6833–46. doi: https://doi.org/10.7150/thno.59020.

[38] He W, Yan J, Li Y, Yan S, Wang S, Hou P, et al. Resurrecting a p53 peptide activator - An enabling nanoengineering strategy for peptide therapeutics. J Control Release 2020;325:293–303. doi: https://doi.org/10.1016/j.jconrel.2020.06.041.

[39] He W, Wang S, Yan J, Qu Y, Jin L, Sui F, et al. Self-assembly of therapeutic peptide into stimuli-responsive clustered nanohybrids for cancer-targeted therapy. Adv Funct Mater 2019;29(10):1807736. doi: https://doi.org/10.1002/adfm.201807736.

[40] Fang J, Nakamura H, Maeda H. The EPR effect: Unique features of tumor blood vessels for drug delivery, factors involved, and limitations and augmentation of the effect. Adv Drug Del Rev 2011;63(3):136–51. doi: https://doi.org/10.1016/j.addr.2010.04.009.

[41] Fang J, Islam W, Maeda H. Exploiting the dynamics of the EPR effect and strategies to improve the therapeutic effects of nanomedicines by using EPR effect enhancers. Adv Drug Del Rev 2020;157:142–60. doi: https://doi.org/10.1016/j.addr.2020.06.005.

[42] Choi HS, Gibbs SL, Lee JH, Kim SH, Ashitate Y, Liu F, et al. Targeted zwitterionic near-infrared fluorophores for improved optical imaging. Nat Biotechnol 2013;31(2):148–53. doi: https://doi.org/10.1038/nbt.2468.

[43] Anderson KG, Stromnes IM, Greenberg PD. Obstacles posed by the tumor microenvironment to T cell activity: a case for synergistic therapies. Cancer Cell 2017;31(3):311–25. doi: https://doi.org/10.1016/j.ccell.2017.02.008.

[44] Kang H, Gravier J, Bao K, Wada H, Lee JH, Baek Y, et al. Renal clearable organic nanocarriers for bioimaging and drug delivery. Adv Mater 2016;28(37):8162–8. doi: https://doi.org/10.1002/adma.201601101.

[45] Xibo Z, Chen Q, Zhou J, Ling D, Qiaolin Z. High-efficient clearable nanoparticles for multi-modal imaging and image-guided cancer therapy. Adv Funct Mater 2018;28(2):1704634. doi: https://doi.org/10.1002/adfm.201704634.

[46] Snider J, Kotlyar M, Saraon P, Yao Z, Jurisica I, Stagljar I. Fundamentals of protein interaction network mapping. Mol Syst Biol 2015;11(12):848. doi: https://doi.org/10.15252/msb.20156351.

[47] Katz C, Levy-Beladev L, Rotem-Bamberger S, Rito T, Rüdiger SGD, Friedler A. Studying protein-protein interactions using peptide arrays. Chem Soc Rev 2011;40(5):2131–45. doi: https://doi.org/10.1039/c0cs00029a.
[48] Neklesa TK, Winkler JD, Crews CM. Targeted protein degradation by PROTACs. Pharmacol Ther 2017;174:138–44. doi: https://doi.org/10.1016/j.pharmthera.2017.02.027.
[49] Salami J, Crews CM. Waste disposal-An attractive strategy for cancer therapy. Science 2017;355(6330):1163–7. doi: https://doi.org/10.1126/science.aam7340.
[50] Au YZ, Wang T, Sigua LH, Qi J. Peptide-Based PROTAC: The Predator of Pathological Proteins. Cell Chem Biol 2020;27(6):637–9. doi: https://doi.org/10.1016/j.chembiol.2020.06.002.
[51] Yan J, Ji F, Yan S, You W, He W. A general-purpose nanohybrid fabricated by polymeric Au(I)-peptide precursor to wake the function of peptide therapeutics. Theranostics 2020;10(19):8513–27.
[52] Vousden KH, Lane DP. p53 in health and disease. Nat Rev Mol Cell Bio 2007;8(4):275–83.
[53] Muller PAJ, Vousden KH. Mutant p53 in cancer: new functions and therapeutic opportunities. Cancer Cell 2014;25(3):304–17. doi: https://doi.org/10.1016/j.ccr.2014.01.021.
[54] Sabapathy K, Lane DP. Therapeutic targeting of p53: all mutants are equal, but some mutants are more equal than others. Nat Rev Clin Oncol 2018;15(1):13–30. doi: https://doi.org/10.1038/nrclinonc.2017.151.
[55] Muñoz-Fontela C, Mandinova A, Aaronson SA, Lee SW. Emerging roles of p53 and other tumour-suppressor genes in immune regulation. Nat Rev Immunol 2016;16(12):741–50. doi: https://doi.org/10.1038/nri.2016.99.
[56] Khan S, He Y, Zhang X, Yuan Y, Pu S, Kong Q, et al. PROteolysis TArgeting Chimeras (PROTACs) as emerging anticancer therapeutics. Oncogene 2020;39(26):4909–24. doi: https://doi.org/10.1038/s41388-020-1336-y.